

Long-Term PM_{2.5} Forecasting Using a DTW-Enhanced CNN-GRU Model

Amirali Ataee Naeini¹, Arshia Ataee Naeini², Fatemeh Karami Mohammadi², and Omid Ghaffarpasand^{3,*}

¹Department of Computer Science, University of California, Davis, Davis CA, USA

²Department of Electrical and Computer Engineering, University of Tehran, Tehran, Iran

³School of Geography, Earth, and Environmental Sciences, University of Birmingham, Birmingham, UK

Abstract. Reliable long-term forecasting of PM_{2.5} concentrations is critical for public health early-warning systems, yet existing deep learning approaches struggle to maintain prediction stability beyond 48 hours, especially in cities with sparse monitoring networks. This paper presents a deep learning framework that combines Dynamic Time Warping (DTW) for intelligent station similarity selection with a CNN-GRU architecture to enable extended-horizon PM_{2.5} forecasting in Isfahan, Iran, a city characterized by complex pollution dynamics and limited monitoring coverage. Unlike existing approaches that rely on computationally intensive transformer models or external simulation tools, our method integrates three key innovations: (i) DTW-based historical sampling to identify similar pollution patterns across peer stations, (ii) a lightweight CNN-GRU architecture augmented with meteorological features, and (iii) a scalable design optimized for sparse networks. Experimental validation using multi-year hourly data from eight monitoring stations demonstrates superior performance compared to state-of-the-art deep learning methods, achieving $R^2 = 0.91$ for 24-hour forecasts. Notably, this is the first study to demonstrate stable 10-day PM_{2.5} forecasting ($R^2 = 0.73$ at 240 hours) without performance degradation, addressing critical early-warning system requirements. The framework's computational efficiency and independence from external tools make it particularly suitable for deployment in resource-constrained urban environments.

Keywords. Air pollution forecast; Deep learning; Dynamic Time Warping; Urban environment, Isfahan.

1. Introduction

Air pollution is one of the most critical environmental challenges of our time, with profound impacts on human health and ecological systems. Among various atmospheric pollutants, fine particulate matter with an aerodynamic diameter of 2.5 micrometers or less, commonly referred to as PM_{2.5}, is recognized as a significant public health concern due to its ability to infiltrate deep into the respiratory and circulatory systems (C.-Y. Chen et al., 2025). According to the World Health Organization (WHO), elevated PM_{2.5} concentrations are strongly correlated with a wide range of adverse health effects, including respiratory diseases such as asthma and chronic bronchitis, cardiovascular diseases, lung cancer, and increased mortality rates (Tsai et al., 2025). Beyond health impacts, PM_{2.5} also contributes to visibility reduction and imposes substantial environmental remediation costs on governments (Talaiekhozani et al., 2017; C. Zhang et al., 2025). The increasing frequency and intensity of significant air pollution events globally underscore the urgent need for effective strategies to mitigate their impacts, providing a crucial reference for people's travel and health protection, and offering a basis for government environmental management.

* Corresponding author; Email. o.ghaffarpasand@bham.ac.uk

Given the serious health and environmental consequences of PM_{2.5} pollution, accurate and timely forecasting is essential for effective environmental management, informed policymaking, and individual health protection. Reliable predictions enable early warning systems, support the implementation of control measures, guide public behaviour, and inform urban planning. Both short-term (hourly to daily) and long-term (multi-day to weekly) forecasts play critical roles, each presenting distinct challenges and offering different benefits for operational and strategic decision-making.

Air quality prediction approaches are generally categorized into deterministic and statistical methods. Deterministic models, such as chemical transport and dispersion models, are grounded in aerodynamic theory, chemical kinetics, and meteorology to simulate the emission, transformation, and transport of pollutants (Byun & Schere, 2006; Y. Zhang et al., 2012). While physically rigorous, these models often depend on theoretical assumptions and limited observational inputs, which can introduce considerable uncertainty, and they typically require substantial computational resources. In contrast, statistical methods adopt data-driven strategies that rely on historical observations to build predictive models, offering greater simplicity and flexibility (Zhu et al., 2022). Widely used techniques include Autoregressive Integrated Moving Average (ARIMA), Support Vector Machines (SVM), Random Forests (RF), Decision Trees (DT), and Multilayer Perceptron's (MLP) (Zhu et al., 2022). More recently, the emergence of deep learning has advanced air quality forecasting, as neural network architectures are capable of modelling complex non-linear and nonstationary temporal dependencies. Empirical studies demonstrate that deep learning models, including feedforward and recurrent neural networks, frequently surpass traditional statistical and deterministic approaches when sufficient data and computational resources are available (X. Li et al., 2016; Zhu et al., 2022).

Several deep learning architectures have been adopted for air quality forecasting. Convolutional Neural Networks (CNNs) are particularly effective for spatial feature extraction, when combined with LSTM networks in hybrid models like ConvLSTM, they can handle and subsample spatiotemporal patterns directly from transformed image-like pollutant data, enabling city-scale air pollution interpolation and prediction (Le et al., 2020). Concurrently, pure LSTM networks and CNN–LSTM hybrids (such as the Deep-AIR framework) excel in time-series forecasting by capturing complex spatial interactions (e.g., road density, urban form) and long-term temporal dependencies, thus substantially improving forecasting accuracy in metropolitan environments (Han et al., 2021). Bidirectional LSTM (BiLSTM) networks, as noted by Shi et al. (2022), process time series data in both forward and reverse sequences, allowing them to capture and integrate information that might be overlooked by unidirectional LSTMs, thereby enhancing the model's learning capability and prediction effectiveness. Gated Recurrent Unit (GRU) networks are also utilized in deep learning models for forecasting decomposed subsequence data, with H. Huang & Qian (2023) proposing an ensemble GRU model incorporating a self-weighted total loss function based on variational mode decomposition (VMD) for optimal predictions. Transformer Networks are lightweight deep learning models designed to learn long-term dependencies and complex relationships from time series data, with Z. Zhang & Zhang (2023) and Z. Zhang et al. (2022) applying Transformer-

based models for daily PM_{2.5} predictions and hourly PM_{2.5} forecasting, often using sparse attention mechanisms to reduce time complexity and improve performance.

Hybrid deep learning models have become an important direction in PM_{2.5} forecasting, aiming to combine the complementary strengths of different architectures for enhanced spatiotemporal prediction. For example, CNN–LSTM hybrids have been applied in Beijing, China, where CNN’s ability to extract spatial features was combined with LSTM’s capacity for temporal dependency modelling (C.-J. Huang & Kuo, 2018; T. Li et al., 2020; Pak et al., 2020). Variants incorporating bidirectional LSTM, attention mechanisms, and signal decomposition techniques such as CEEMDAN have demonstrated further gains in multi-site, multi-horizon forecasting across different regions of China, including Beijing (Y. Chen et al., 2021; D. Li et al., 2022), Hangzhou and Kunming (Ban & Shen, 2022), and other Chinese cities (Zeng et al., 2023). Transformer-based models, including sparse attention architectures and temporal difference graph networks, have been evaluated in Beijing and Taizhou, China (Z. Zhang et al., 2022; Z. Zhang & Zhang, 2023), showing strong capability in capturing long-range dependencies. Graph Neural Network (GNN) hybrids, such as GCN–LSTM and multi-graph approaches, have been widely used in China as well, including studies in the Beijing-Tainjin-Hebei region (Qi et al., 2019), Haidian district of Beijing (H. Wang et al., 2023) and broader Chinese networks (M. Wu et al., 2025). Additional strategies, such as CNN–ensemble models evaluated in Kaohsiung, Taiwan (M.-H. Chen et al., 2023) and meteorological decomposition-based approaches (Y.-C. Chen & Li, 2021), further highlight the diversity of hybrid architectures explored across East Asia.

However, despite these advancements, many PM_{2.5} forecasting models still struggle to capture long-term and complex temporal dependencies, particularly in regions with sparse monitoring networks (Kaveh et al., 2025; C. Wu et al., 2025). A major limitation is that most approaches emphasize single-station temporal dynamics while neglecting spatial correlations and cross-site dependencies (Y. Wang et al., 2024). Moreover, hybrid or multi-component models often underperform when sub-models operate independently on different parts of the signal without effective integration, yielding only modest accuracy gains (Jia et al., 2025). External factors such as meteorological variability and seasonal cycles are also frequently underutilized, reducing the robustness of predictions (Jia et al., 2025). Deep learning methods, while powerful, can have difficulty capturing linear trend components and may become computationally inefficient when combined with decomposition techniques. Similarly, complex encoder–decoder frameworks require extensive hyperparameter tuning to achieve optimal performance (Zhou et al., 2024). These challenges are especially pronounced in data-scarce regions, where limited historical records and sparse monitoring networks constrain model training and generalizability (Kaveh et al., 2025; C. Wu et al., 2025).

Given this context, AI-based forecasting frameworks have significant untapped potential for improving air quality prediction in data-sparse urban environments, yet research in this area remains scarce. To address this gap, we focus on Isfahan, the Iran’s third-largest city and a prime example of the forecasting challenges posed by limited monitoring density, heterogeneous emission sources, and complex meteorological regimes. Located in a semi-arid basin surrounded by the Zagros Mountains, Isfahan frequently experiences winter inversions

and restricted vertical mixing, leading to persistent pollution episodes. The city's emission landscape spanning industrial hubs, congested traffic corridors, and residential areas, produces highly variable spatial and temporal pollution patterns, further complicating forecasting efforts (Hosseiniebalam & Ghaffarpasand, 2015).

To meet these challenges, we propose a deep learning framework that integrates spatial, temporal, and meteorological dimensions into a unified prediction model. Our approach employs a hybrid 2D CNN–GRU architecture, where convolutional layers extract spatial features from dynamically selected peer stations, identified using Dynamic Time Warping (DTW), and GRU layers model temporal dependencies across multiple forecast horizons. Auxiliary meteorological variables, including wind speed, wind direction, and temperature, are incorporated to provide context for pollutant dispersion and accumulation. Unlike conventional distance-based proximity measures, our similarity-driven approach allows the model to learn from both geographically near and remote stations with comparable temporal patterns, improving generalization across heterogeneous atmospheric regimes. Our design is inspired by the 3D CNN–GRU model developed previously by Faraji et al. (2022), which used DTW-based station similarity for short-term prediction in Tehran, capital of Iran. However, we extend this approach to longer forecasting horizons and explicitly evaluate performance at unmonitored stations. Furthermore, by applying the method to Isfahan, a semi-arid basin city with frequent winter inversions and limited monitoring, we test its robustness in a significantly different environmental and topographical context, contrasting with Tehran's urban pollution regime.

2. Proposed Model

Convolutional neural networks (CNNs) are deep feed-forward architectures originally developed for visual pattern recognition (LeCun & Bengio, 1998). By applying convolution operations with localized kernels and shared weights, CNNs extract salient features that capture local patterns in data. In a typical 2D convolution, a kernel of size $H \times W$ is slid over the input to produce feature maps via weighted sums:

$$y_{i,j}^{(k)} = \sum_{c=1}^{C_{\text{in}}} \sum_{u=1}^H \sum_{v=1}^W W_{c,u,v}^{(k)} x_{c,i+u-1,j+v-1} + b^{(k)} \quad (1)$$

where $W^{(k)}$ is the filter for output channel k and $b^{(k)}$ is a bias term. This operation endows CNNs with translational invariance and efficient feature sharing. In time series forecasting, CNNs are leveraged to model short-term temporal patterns by treating the time axis (and possibly multiple variables) analogously to spatial dimensions, thereby detecting local dependencies and trends in the sequence data.

Gated Recurrent Units (GRUs) are a recurrent network architecture introduced as a simpler gating-based variant of recurrent neural networks (Cho et al., 2014). A GRU maintains a hidden state h_t that evolves over time, using an update gate z_t and a reset gate r_t to control information flow. These gates are defined by sigmoid activations and govern how the previous state h_{t-1} and current input x_t are blended to compute the new state. In particular, the gating mechanism can be described as:

$$z_t = \sigma(W_z x_t + U_z h_{t-1} + b_z), \quad (2)$$

$$r_t = \sigma(W_r x_t + U_r h_{t-1} + b_r), \quad (3)$$

$$\tilde{h}_t = \tanh(W_h x_t + U_h (r_t \odot h_{t-1}) + b_h), \quad (4)$$

$$h_t = z_t \odot h_{t-1} + (1 - z_t) \odot \tilde{h}_t \quad (5)$$

where $z_t \in (0,1)^e$ and $r_t \in (0,1)^e$ are element-wise gate vectors (with e the dimension of the hidden state), and W_*, U_*, b_* are learned parameters. The update gate z_t dictates the extent to which the previous hidden state is retained (when z_t is close to 1, most of h_{t-1} is kept), while the reset gate r_t controls how much of the past state is used in computing the candidate state \tilde{h}_t . This gating mechanism enables GRUs to capture long-term temporal dependencies and alleviate vanishing gradient issues, similar to LSTMs but with fewer parameters (Cho et al., 2014). In time series forecasting, GRU-based models excel at sequence modeling by adaptively learning what information to remember or forget over time. Notably, hybrid architectures that combine CNN and GRU layers have shown improved forecasting accuracy by leveraging CNNs for short-term feature extraction and GRUs for modeling sequential dynamics (LeCun & Bengio, 1998; J. Wang et al., 2023). Such CNN-GRU models capitalize on CNNs' ability to detect local temporal patterns and GRUs' strength in preserving long-range dependencies, thereby providing a powerful framework for complex temporal data forecasting.

2.1. Model Design

We denote the hourly PM_{2.5} concentration observed at station s_i and time t by $x_{i,t} \in \mathbb{R}$. Let

$x_{i,t}^\tau = [x_{i,t-\tau+1}, \dots, x_{i,t}]^\top \in \mathbb{R}^\tau$ be the τ -length backward window that will serve as the predictive context. For each target station s_i we construct a spatio-temporal tensor

$$\mathcal{X}_{i,t} = \left[x_{j,t}^{(\tau)} \right]_{j \in \mathcal{N}_i} \in \mathbb{R}^{\tau \times |\mathcal{N}_i|}, \quad (6)$$

where \mathcal{N}_i denotes a dynamically selected set of “peer” stations obtained via DTW (Section 2.1.1). The tensor is reshaped to $X_{i,t} \in \mathbb{R}^{1 \times |\mathcal{N}_i| \times \tau}$ so that the first dimension represents a single input channel.

2D CNN-GRU backbone. The backbone maps $X_{i,t}$ to a hidden representation $\mathbf{h}_{i,t} \in \mathbb{R}^{d_h}$ through a composition

$$\mathbf{h}_{i,t} = \phi \circ \underbrace{\text{GRU}_{\theta_g}}_{L_g \text{ layers}} \circ \underbrace{\text{CNN}_{\theta_c}}_{L_c \text{ layers}} (X_{i,t}), \quad (7)$$

where θ_g and θ_c are trainable parameters, CNN consists of L_c 2-D convolutional layers with kernel $\mathbf{W}^{(c)} \in \mathbb{R}^{k_h \times k_w \times C_{\text{in}} \times C_{\text{out}}}$ followed by SeLU activations, and ϕ denotes layer normalization. Convolution is performed over the $(|\mathcal{N}_i|, \tau)$ plane to fuse the spatially pooled series:

$$\mathbf{Z}^{(c)} = \sigma(\mathbf{W}^{(c)} * \mathbf{X}_{i,t} + b^{(c)}) \in \mathbb{R}^{|\mathcal{N}_i| \times \tau \times C_{\text{out}}}. \quad (8)$$

The resulting feature cube is flattened across the spatial dimension and fed into a stacked GRU, which updates its hidden state via

$$\mathbf{z}_t = \sigma(\mathbf{W}_z[\mathbf{x}_t, \mathbf{h}_{t-1}] + \mathbf{b}_z), \quad (9)$$

$$\mathbf{r}_t = \sigma(\mathbf{W}_r[\mathbf{x}_t, \mathbf{h}_{t-1}] + \mathbf{b}_r), \quad (10)$$

$$\tilde{\mathbf{h}}_t = \tanh(\mathbf{W}_h[\mathbf{x}_t, \mathbf{r}_t \odot \mathbf{h}_{t-1}] + \mathbf{b}_h), \quad (11)$$

$$\mathbf{h}_t = (1 - \mathbf{z}_t) \odot \mathbf{h}_{t-1} + \mathbf{z}_t \odot \tilde{\mathbf{h}}_t, \quad (12)$$

with gate vectors $\mathbf{z}_t, \mathbf{r}_t \in (0,1)^{d_h}$ (Faraji et al., 2022). Two GRU blocks ($L_g = 2$) are stacked, each containing $d_h = 256$ units and interleaved with dropout ($p = 0.2$).

- 1) *Dynamic Time Warping Analysis*: For every pair (s_i, s_j) we compute the classical DTW distance $d_{\text{DTW}}(i, j) = \min_{\pi} \sum_{(\alpha, \beta) \in \pi} \|x_{i, \alpha} - x_{j, \beta}\|_2$, where π ranges over all monotone alignment paths of length $\ell \leq \tau$. The *peer set* \mathcal{N}_i is then defined as

$$\mathcal{N}_i = \{s_i\} \cup \arg \min_{\substack{\mathcal{S} \subseteq V \setminus \{i\} \\ |\mathcal{S}|=K-1}} \sum_{j \in \mathcal{S}} d_{\text{DTW}}(i, j), \quad (13)$$

with $K = 5$ in all experiments. This criterion maximizes temporal-pattern affinity irrespective of Euclidean distance or prevailing wind vector, yielding a more informative spatial context than purely geographical neighbors. This approach has been proven effective in previous air pollution prediction models (Faraji et al., 2022).

- 2) *2D CNN and GRU Layers*: Equation (8) employs rectangular kernels $(k_h, k_w) = (|\mathcal{N}_i|, 3)$ so that each filter convolves across the entire peer set while sliding along the temporal axis. Let $\mathbf{F} \in \mathbb{R}^{d_f \times \tau'}$ denote the flattened output after L_c layers. The GRU treats each column $\mathbf{f}_t \in \mathbb{R}^{d_f}$ as the sequential input at step t ($t = 1, \dots, \tau'$), thereby disentangling local temporal motifs from cross-station dependencies learned by the CNN.
- 3) *Meteorological Auxiliary Data Input*: We augment $\mathbf{h}_{i,t}$ with a meteorological embedding $\mathbf{m}_t \in \mathbb{R}^{d_m}$ obtained from the raw meteorological triplet $\mathbf{w}_t = [\text{WS}, \text{WD}, \text{Temp}]^\top \in \mathbb{R}^3$ via a two-layer perceptron:

$$\mathbf{m}_t = \rho(\mathbf{W}_2 \rho(\mathbf{W}_1 \mathbf{w}_t + \mathbf{b}_1) + \mathbf{b}_2) \quad (14)$$

$$\rho(x) = \max(0, x) \quad (15)$$

The concatenated vector $\tilde{\mathbf{h}}_{i,t} = [\mathbf{h}_{i,t}; \mathbf{m}_t] \in \mathbb{R}^{d_h + d_m}$ is regularized through batch normalization before prediction.

- 4) *Output Layer*: Let $H = d_h + d_m$. A regression head $\psi: \mathbb{R}^H \rightarrow \mathbb{R}^{H_o}$ with parameters $\mathbf{W}_o \in \mathbb{R}^{H_o} \times H$ and bias \mathbf{b}_o maps

$$\hat{\mathbf{y}}_{i,t+q} = \mathbf{W}_o \tilde{\mathbf{h}}_{i,t} + \mathbf{b}_o, \quad q = 1, \dots, Q, \quad (16)$$

where Q is the forecast horizon (here $Q = 6$). For multi-step prediction we adopt *direct strategy*: the head outputs $H_0 = Q$ scalars representing $\hat{x}_{i,t+1}, \dots, \hat{x}_{i,t+Q}$ simultaneously, avoiding exposure bias inherent in recursive roll-outs. The architecture of the proposed CNN–GRU model, shown in Figure 1, integrates a spatiotemporal input tensor where $Sims$ denotes the number of similar states selected via DTW, ns represents the number of states, and t corresponds to the time lag used to capture temporal dependencies.

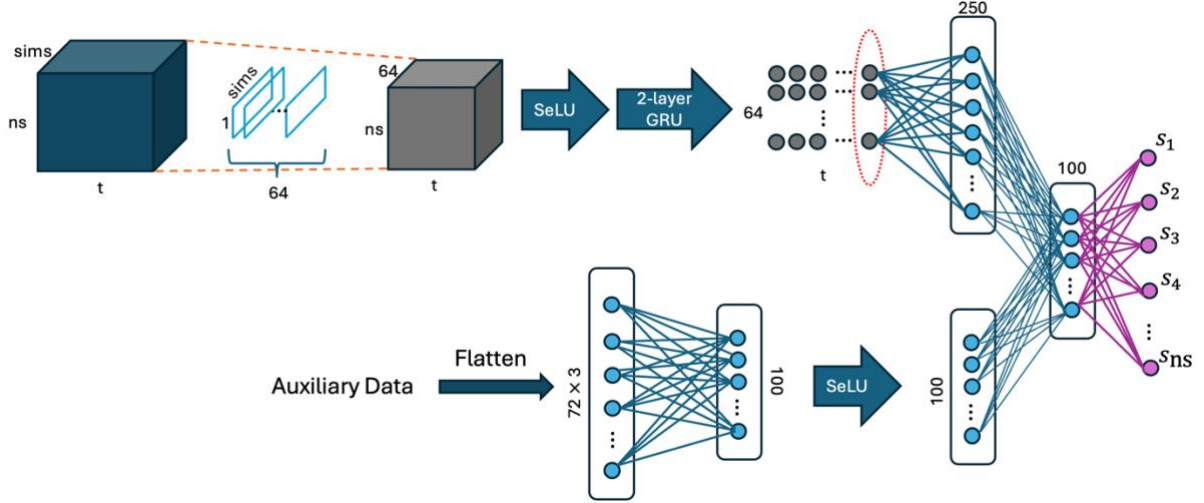


Figure 1. Schematic architecture of the proposed spatiotemporal forecasting CNN–GRU model.

2.2. Model Validation

In supervised learning, data partitioning plays a critical role in balancing model training and evaluation. A substantial portion of the dataset is typically allocated to training in order to capture underlying patterns, while smaller portions are reserved for validation and testing to assess generalization (Maloof & others, 2006). Overly small training sets may hinder convergence, whereas excessively large ones can lead to optimistic accuracy estimates and reduced reliability (Xu & Goodacre, 2018). To maintain this balance, the present study assigns 60% of the data to training, 20% to validation for model tuning, and the remaining 20% to independent testing. Given the predicted sequence $\hat{\mathbf{x}}_{i,t}^{(Q)}$ and the ground-truth $\mathbf{x}_{i,t}^{(Q)}$, we compute:

(a) Mean Absolute Error

$$MAE = \frac{1}{nQ} \sum_{i,t,q} |\hat{x}_{i,t+q} - x_{i,t+q}|. \quad (17)$$

(b) Root Mean Squared Error

$$\text{RMSE} = \sqrt{\frac{1}{nQ} \sum_{i,t,q} (\hat{x}_{i,t+q} - x_{i,t+q})^2}. \quad (18)$$

(c) Coefficient of Determination

$$R^2 = 1 - \frac{\sum_{i,t,q} (\hat{x}_{i,t+q} - x_{i,t+q})^2}{\sum_{i,t,q} (x_{i,t+q} - \bar{x})^2}, \quad (19)$$

$$\bar{x} = \frac{1}{nQ} \sum_{i,t,q} x_{i,t+q}. \quad (20)$$

Training minimizes the scale-invariant *mean squared logarithmic error* (MSLE),

$$\mathcal{L} = \frac{1}{nQ} \sum_{i,t,q} (\ln(1 + \hat{x}_{i,t+q}) - \ln(1 + x_{i,t+q}))^2, \quad (21)$$

which penalizes fractional deviations more heavily at lower concentrations. Optimization is performed with AdamW ($\eta = 4 \times 10^{-4}$, weight-decay 10^{-4}) for 800 epochs; early stopping (patience 20 epochs) is triggered on the validation MSLE. All layers are initialized with He-normal scheme; gradient norms are clipped to 5 to stabilize training.

3. Implementation

3.1. Study Area

Isfahan, located at approximately $32^{\circ}39'N, 51^{\circ}40'E$, is a major urban and industrial centre in central Iran and the capital of Isfahan Province. With a population exceeding 2 million, it is Iran's third-largest city. Isfahan lies at an elevation of roughly 1,570 m above sea level within a semi-arid plateau, receiving under 150 mm of annual precipitation (Jadidi et al., 2019). The city is bordered to the west by the Zagros Mountains, whose orographic barrier, in combination with the basin topography and frequent winter temperature inversions, reduces atmospheric mixing and intensifies pollutant accumulation (Abadi et al., 2025).

Ambient air pollution, particularly $\text{PM}_{2.5}$ has emerged as one of Isfahan's most critical environmental and public health challenges. Observational data suggest that annual average $\text{PM}_{2.5}$ concentrations in the city typically exceed $30 \mu\text{g}/\text{m}^3$, which is over three times the WHO-recommended threshold of $10 \mu\text{g}/\text{m}^3$ (Abadi et al., 2025; Jadidi et al., 2019; Soleimani & et al., 2022). In some years, concentrations have surpassed $70 \mu\text{g}/\text{m}^3$ during prolonged pollution episodes (Sohrabi & Maleki, 2025). Key emission sources include high vehicular density, petrochemical and steel industries, residential biomass burning, and natural dust intrusions from surrounding arid regions (Abadi et al., 2025).

Exposure to elevated $\text{PM}_{2.5}$ levels has been strongly associated with increased rates of cardiovascular and respiratory disease and reduced life expectancy in Isfahan. Long-term epidemiological studies report a statistically significant association between each $10 \mu\text{g}/\text{m}^3$ increase in $\text{PM}_{2.5}$ and a 3 – 5% increase in cardiopulmonary events (Faridi et al., 2022;

Soleimani & et al., 2022). These impacts are particularly severe during winter months, when inversion layers trap pollutants near the surface.

To monitor air quality, the Isfahan Department of Environment maintains a network of thirteen automated stations across the city. These stations capture hourly concentrations of PM_{2.5} and other pollutants, as well as meteorological parameters such as wind speed, wind direction, temperature, and humidity (Jadidi et al., 2019). For the current study, five stations with over 30% missing or unreliable data were excluded, resulting in a dataset composed of eight high-quality stations. These stations cover a range of land uses, including residential neighbourhoods, industrial districts, and traffic-heavy corridors, ensuring spatial representativeness of the urban atmosphere.

In addition to PM_{2.5}, three key meteorological variables, wind speed, wind direction, and temperature, were used as auxiliary inputs. These hourly features were synchronized with PM_{2.5} measurements and appended to the deep learning model to account for short-term dispersion and atmospheric transport dynamics.

Given the spatial heterogeneity of emission sources and microclimatic patterns in Isfahan, we employed a Dynamic Time Warping (DTW) approach to identify the most temporally correlated stations for each prediction target. This similarity-based pooling method allows the model to learn from both proximate and remote but statistically similar stations, enhancing predictive generalization across varying atmospheric regimes.

3.2. Data Description

We collected hourly PM_{2.5} concentration data from eight air quality monitoring stations across Isfahan from 2018 to 2023. In addition to pollutant measurements, we incorporated three meteorological variables: air temperature, wind speed, and wind direction, as these factors have been shown to strongly influence the dispersion, transport, and accumulation of PM_{2.5} in urban environments (Karimian et al., 2019; Mohammadi et al., 2024; Salehi et al., 2021). These data were obtained from meteorological stations co-located with the air quality monitoring sites.

Figure 2 presents the distributions of these meteorological parameters across all stations. The solid line in each subplot represents the Kernel Density Estimate (KDE), which provides a smoothed, continuous approximation of the data's underlying probability density. The KDE complements the histogram by highlighting the general shape and continuity of the distribution without being constrained by bin size. As shown, air temperature exhibits a near-normal distribution centered around moderate values, reflecting the region's temperate conditions. Wind direction displays a bimodal tendency, suggesting dominant prevailing wind flows from two principal directions, while wind speed shows a right-skewed distribution with most observations clustered around 2–3 m/s and fewer instances of higher speeds. These patterns collectively indicate relatively stable meteorological conditions, with moderate winds contributing to pollutant accumulation episodes during stagnant periods.

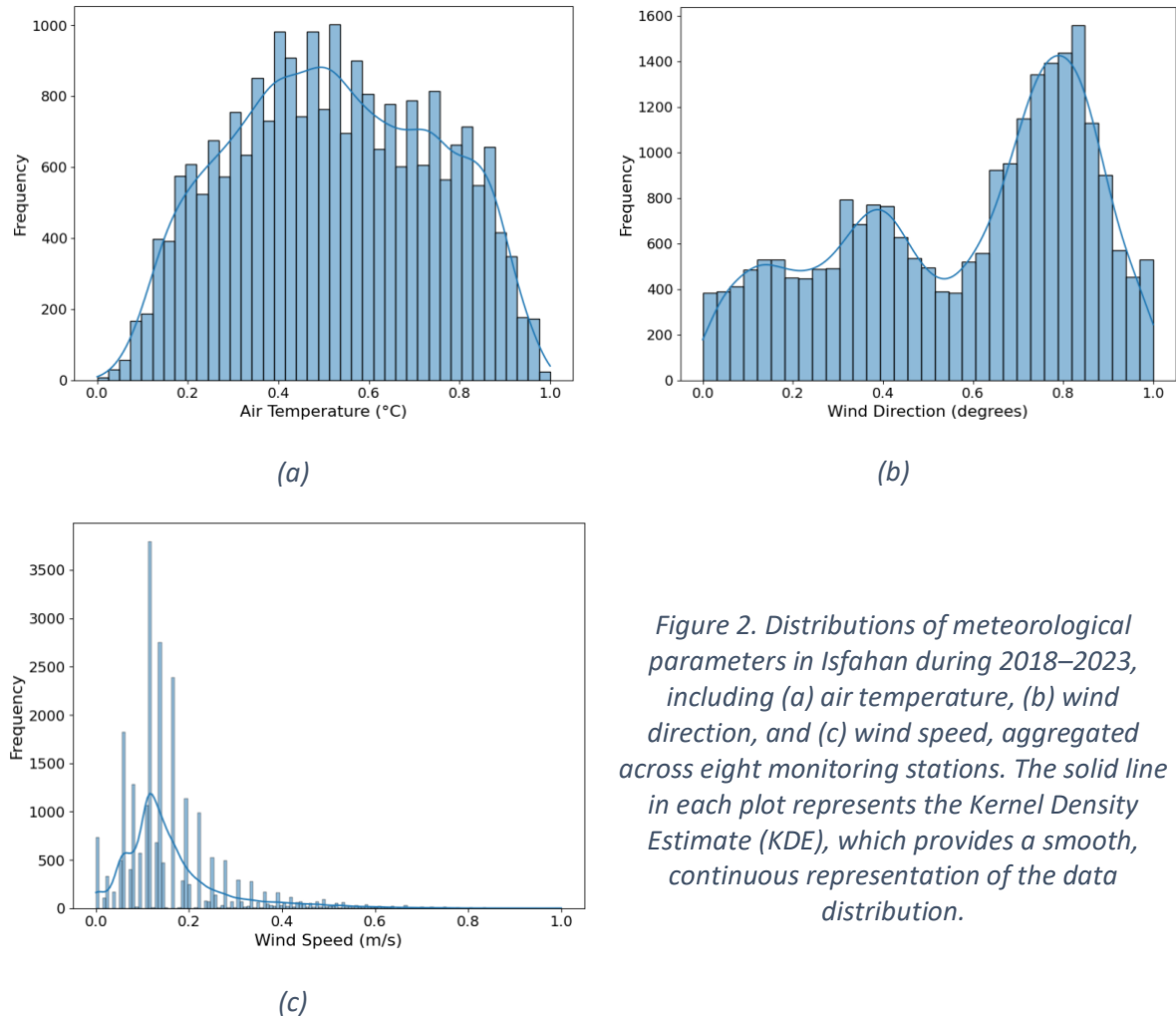


Figure 2. Distributions of meteorological parameters in Isfahan during 2018–2023, including (a) air temperature, (b) wind direction, and (c) wind speed, aggregated across eight monitoring stations. The solid line in each plot represents the Kernel Density Estimate (KDE), which provides a smooth, continuous representation of the data distribution.

3.3. Data Preprocessing

To ensure the reliability and consistency of the training and testing processes, a detailed data preprocessing strategy was employed prior to model development. Hourly PM_{2.5} concentration records from 13 monitoring stations in Isfahan were initially collected. After a thorough inspection of data availability and quality, five stations exhibiting excessive missing values or low data continuity were excluded from the study. The remaining eight stations provided sufficient data coverage for both temporal modeling and inter-station similarity computation.

For each station, PM_{2.5} measurements were aligned into a unified hourly time index to maintain consistent temporal sequencing across stations. Missing data within each station's PM_{2.5} time series were handled using a two-tier imputation strategy. For short and sporadic gaps, forward-fill and backward-fill techniques were applied, replacing missing values with the most recent or subsequent available observations. These methods have been shown to be effective for short-term missingness in environmental time series, where adjacent values are highly correlated (Karnati et al., 2025; Lee et al., 2025). This approach ensures continuity without imposing strong distributional assumptions. In contrast, longer or irregular gaps, particularly those occurring near the temporal boundaries of the series, were left unfilled. Over-extending

carry-forward or carry-backward imputations across large gaps can artificially suppress variability and introduce bias, especially when temporal support is lacking on one side (Lee et al., 2025; Mike Nguyen, 2023). Therefore, these segments were retained as missing to preserve the integrity of the temporal signal, following the recommendation that aggressive imputation in poorly supported contexts may distort trends and reduce model reliability (Mike Nguyen, 2023).

To facilitate similarity modelling, inter-station similarity was defined in terms of the alignment of temporal patterns in $PM_{2.5}$ concentrations. Specifically, Dynamic Time Warping (DTW) was employed to compute pairwise distance matrices over normalized hourly time windows, where smaller DTW distances indicate greater similarity in pollutant dynamics. This approach has been widely adopted in air quality studies to capture shape-based similarities in time series, overcoming limitations of simple Euclidean measures (Faraji et al., 2022; Suris et al., 2022). For each target station, the five most similar stations were selected according to their DTW scores, and these were used to construct a structured spatiotemporal input tensor of dimension (N, M, r) , where $N = 8$ is the number of target stations, $M = 5$ is the number of DTW-selected similar stations (including the target itself), and $r = 12$ denotes the number of time lags.

In parallel, auxiliary meteorological variables including wind speed, wind direction, and ambient temperature, were collected on an hourly basis from the meteorological stations co-located with each air quality monitoring site in Isfahan. These variables were time-synchronized with the air quality data and arranged into a matrix of shape $(t, 3)$, where t is the number of hourly records. These auxiliary inputs were used to provide external atmospheric context to the temporal evolution of $PM_{2.5}$ concentrations. All numeric features ($PM_{2.5}$ and auxiliary variables) were normalized using min-max scaling to a range of $[0, 1]$. Normalization was performed independently on the training set and subsequently applied to validation and test sets using the same scaling parameters to prevent data leakage. We then adopted a sliding window technique to convert the normalized time series into input-output sequences. Each input sequence consisted of 72 historical hours of $PM_{2.5}$ and auxiliary features. These sequences were paired with output windows ranging from 8 to 240 hours for prediction. The sliding window advanced hour by hour to maximize the number of training samples and retain temporal structure.

To model spatial relationships, we augmented each target station's input with data from its three most similar stations. Similarity was determined using either geographic distance or correlation-based similarity scores computed on historical pollution levels. The final model input took the form of a multi-channel tensor, allowing it to learn spatial patterns in addition to temporal dependencies. Lastly, for temporal robustness, we introduced a similarity-based historical sampling technique. For each input sequence, we retrieved four past sequences with the most similar temporal structures. These sequences were appended to the input to guide the model using historical analogs, thereby enhancing performance especially for medium- and long-range forecasts.

3.4. Experimental Settings

The implementation was conducted using the PyTorch framework on a Google Colab environment with GPU acceleration. The dataset was split into training (60%), validation (20%), and test (20%) subsets. Input sequences consisted of 72-hour histories of PM_{2.5} concentrations for each station, along with auxiliary meteorological features for the same period. Each training instance was constructed by assembling the current station and its five most similar counterparts, identified through DTW analysis, forming a (8, 5, 12) input tensor per batch. For each instance, the prediction target was the PM_{2.5} values over the next 5 hours for all 8 stations, resulting in a (8, 5) label tensor.

The CNN layer, comprising 64 filters, was used to extract spatial patterns from the input tensor. Its output was reshaped and passed into a two-layer GRU network, each with 48 hidden units. The GRU network is responsible for modelling long-term temporal dependencies and avoiding vanishing gradients. After temporal modelling, the output was concatenated with auxiliary meteorological variables (air temperature, wind speed, and wind direction), which were also normalized beforehand.

The model architecture consisted of a 2D convolutional layer (kernel size = (1, 5), channels = 64), followed by a two-layer GRU network (hidden size = 250). The CNN output was reshaped and fed into the GRU to model temporal dependencies. Auxiliary meteorological input of shape (72, 3) was flattened and passed through two fully connected layers with 128 and 64 units, respectively, reducing it to a 100-dimensional feature vector. Dropout regularization was applied with a rate of 0.2, and ReLU was used as the activation function throughout the network. The model was trained using the Adam optimizer with a learning rate of 0.001 and early stopping criteria with a patience of 5 epochs. This auxiliary representation was concatenated with the GRU output before passing through a final dense layer for prediction. The network was trained using the Mean Squared Error (MSE) loss function and optimized via stochastic gradient descent with momentum.

To test the model's robustness across different forecast horizons, we extended the model to predict PM_{2.5} levels every 8 hours up to one week (i.e., 1, 8, 16, ..., 168 hours ahead). Each model was trained separately using the same input configuration but with adjusted labels for the corresponding forecast lead time. Evaluation was conducted using R², RMSE, and MAE metrics on the test set for each horizon, and performance was further analyzed across low-, medium-, and high-pollution episodes by partitioning the test samples based on observed concentration levels. The key hyperparameters, training configuration, and computational environment used in these experiments are summarized in Table 1.

Table 1. Configuration and optimized hyperparameters of the proposed CNN–GRU model used for multi-horizon PM_{2.5} forecasting.

Parameter	Value
Framework	PyTorch 2.0
Optimizer	Adam
Learning Rate	0.001
Batch Size	64
Dropout Rate	0.2
Epochs	45
CNN Output Channels	64
GRU Layers	2
GRU Hidden Units	48
Fully Connected Layers	2 (128 and 64 units)
Activation Function	ReLU
Normalization	Min-Max normalization
Similarity Sample Size	4
Early Stopping	Patience = 5
Hardware	Google Colab GPU

3.5. Model Evaluation

To evaluate the performance of the proposed model, five state-of-the-art deep learning methods for air pollution prediction namely 3D CNN-GRU, CNN-BiLSTM + Attention, AirFormer, CNN-LSTM, and TS-LSTM are examined. These models represent various strategies in modeling spatiotemporal pollutant dynamics and integrating meteorological context.

Faraji et al. (2022) proposed an integrated 3D CNN-GRU deep learning framework for short-term PM_{2.5} forecasting in Tehran, Iran. Their approach combines a 3D convolutional layer to capture spatial dependencies across air quality monitoring stations with GRU layers for modelling temporal dynamics. To enhance spatial learning, stations with similar PM_{2.5} trends were identified using Dynamic Time Warping (DTW) instead of relying solely on geographical proximity. The model also incorporates meteorological variables as auxiliary input and outperformed several baselines, including GRU, LSTM, ANN, SVR, and ARIMA. It achieved an R² of 0.84 for 1-hour and 0.78 for 24-hour forecasts, demonstrating superior accuracy in both short and extended horizons.

Y. Chen et al. (2021) proposed an attention-enhanced hybrid model combining 1D convolutional neural networks (CNNs) and bidirectional long short-term memory networks (BiLSTM) to predict short-term air pollutant concentrations in Xining, China. The CNN layers extract local temporal features from the input sequence, which are then passed through BiLSTM layers to capture forward and backward dependencies in the time series. An attention mechanism is applied to weigh the contribution of each time step, improving the model's focus on influential patterns. The model integrates both pollutant concentration and meteorological variables, with extensive preprocessing and correlation analysis to select effective features. Evaluation over a five-year dataset demonstrates strong performance, especially for PM_{2.5}, achieving an R² of 0.92 on 24-hour forecasts.

Y. Liang et al. (2023) proposed AirFormer which is a transformer-based model designed to forecast nationwide air quality across China with fine spatial granularity. It introduces a two-stage architecture consisting of a deterministic bottom-up stage and a stochastic top-down stage. In the deterministic phase, novel multi-head self-attention mechanisms, Dartboard Spatial MSA (DS-MSA) and Causal Temporal MSA (CT-MSA) are employed to efficiently capture spatial and temporal dependencies. The stochastic stage enhances predictive robustness by incorporating hierarchical latent variables to model uncertainty. AirFormer was trained on a large-scale dataset covering 1,085 stations and evaluated for 72-hour PM_{2.5} forecasts. It demonstrated significant performance gains, achieving an R² of 0.82 for 24-hour predictions and 0.71 for 72-hour forecasts, outperforming prior deep learning and attention-based baselines.

Mao et al. (2021) introduced a novel TS-LSTME (Temporal Sliding – Long Short-Term Memory Extended) model that leverages spatiotemporal correlations and meteorological auxiliary data for long-term PM_{2.5} forecasting. The model employs a bidirectional LSTM architecture with temporal sliding windows and auxiliary meteorological and temporal features to forecast 24h, 48h, and 72h average PM_{2.5} concentrations across 13 cities in China's Jing-Jin-Ji region. By integrating optimal time lags for prediction blocks, the TS-LSTME outperformed baseline models such as LSTM, LSTME, SVR, and MLR. The model demonstrated strong accuracy with an average R² of 0.87 for 24-hour predictions and maintained competitive accuracy with R² = 0.81 for 72-hour predictions in Beijing, confirming its robustness for extended forecasts.

Tsokov et al. (2022) proposed a hybrid spatiotemporal deep learning framework combining 2D Convolutional Neural Networks (CNNs) and Long Short-Term Memory (LSTM) units for hourly PM_{2.5} forecasting. The model takes into account both local and neighboring station data, incorporating spatial information as image-like inputs and temporal dependencies through LSTM layers. The model's hyperparameters, including input variable subsets, architecture, and convolutional settings are optimized using a genetic algorithm with a customized crossover operator. Additionally, a hybrid missing value imputation method is applied to improve robustness. The final model achieves consistent and competitive results across three Beijing stations, with its best performance at Wanliu station (MAE = 16.75, R² = 0.894). These benchmark models highlight a spectrum of design paradigms for spatiotemporal pollutant forecasting. Each contributes key insights into effective learning strategies for air quality prediction.

4. Results, Discussions, and Limitations

4.1. Model convergence and generalization capability

The training dynamics of the proposed CNN-GRU architecture are depicted in Figure 3, where the training and validation loss trajectories are plotted over 45 epochs. Both curves show a rapid decline during the initial 10 epochs, reflecting the model's ability to quickly learn meaningful spatiotemporal features from the multi-station time series and auxiliary meteorological data. The sharp early improvement suggests that the combination of convolutional layers and recurrent units effectively captures both local spatial dependencies and long-term temporal patterns. As training progresses, the loss values continue to decrease

gradually and eventually stabilize. The training loss converges around 0.04, while the validation loss plateaus slightly above this value, indicating minimal overfitting and strong generalization performance on unseen data.

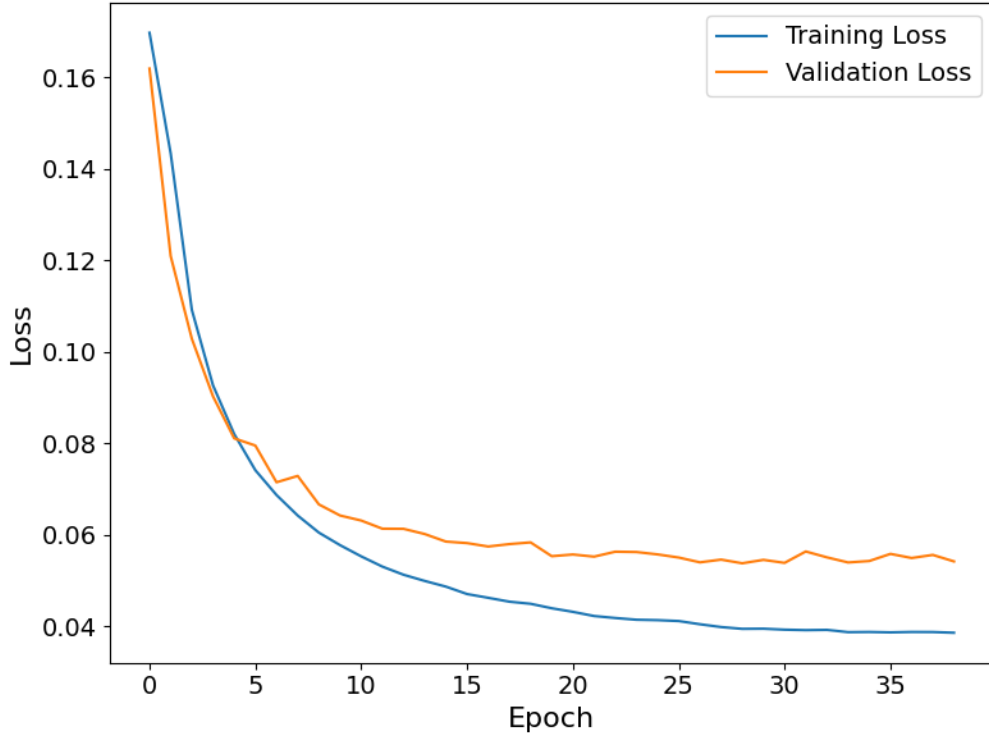


Figure 3. Training and validation loss of the proposed CNN–GRU model over the epochs.

This convergence behaviour validates the effectiveness of our training strategy and model architecture. The inclusion of dropout layers with a rate of 0.2 and an early stopping criterion (patience = 5) played a critical role in avoiding overfitting. Furthermore, the normalization of $\text{PM}_{2.5}$ and auxiliary features via Min-Max standardization contributed to smoother gradient flow and faster convergence. Another important factor was the use of similarity-based historical sampling, which enhanced the model’s capacity to identify relevant patterns from past observations, especially under non-stationary temporal conditions.

4.2. Forecasting Performance Across Horizons

The predictive accuracy of the proposed CNN-GRU framework was evaluated across multiple forecast horizons ranging from 8 to 240 hours using R^2 as the performance metric. As illustrated in Figure 4, the model demonstrates consistently strong performance for short-term forecasts (8–48 hours), achieving average R^2 values above 0.85 across most monitoring stations. This performance reflects the model’s capacity to effectively extract meaningful spatial-temporal patterns from the $\text{PM}_{2.5}$ and auxiliary meteorological data. The high short-term accuracy is further enhanced by the similarity-based historical sampling strategy, which

allows the model to leverage structurally relevant historical sequences, boosting prediction stability.

For mid-range forecasts (72–120 hours), the model maintains a high degree of predictive reliability. At the 120-hour mark, R^2 scores remain above 0.80 at the majority of stations, with some (e.g., Stations 4, 6, and 8) reaching values close to or exceeding 0.90. This indicates that the GRU layers successfully model long-term temporal dependencies, even in the presence of complex meteorological fluctuations. Forecasting accuracy gradually declines beyond 120 hours, a trend consistent with the increasing uncertainty in air quality dynamics and absence of future meteorological variables in the model input. At the furthest horizons (192–240 hours), a more noticeable drop is observed; however, R^2 values above 0.70 are still retained in several stations, indicating acceptable long-range performance.

4.3. Station-wise Performance and Spatial Variability

Despite the overall robust performance of the proposed CNN–GRU framework, the R^2 scores across individual stations reveal meaningful spatial variability. As shown in Figure 4, Stations 1, 4, 6, and 8 consistently achieve high forecasting accuracy, maintaining R^2 values above 0.90 for horizons up to 120 hours. These stations are located in zones with more stable air quality dynamics, likely due to residential zoning, low industrial emissions, and fewer microclimatic disturbances. Similar findings were reported by M. Wu et al. (2025), who observed that models perform better at stations surrounded by uniform land use and meteorological patterns, where pollutant behaviour is more predictable.

In contrast, Station 7 shows notably weaker performance, with R^2 values dropping below 0.65 beyond the 96-hour mark and demonstrating higher variability across all forecast windows. This station is situated near a major highway and adjacent to light industrial activity, introducing localized emission spikes and complex dispersion behaviour. Similar issues were highlighted by Tsokov et al. (2022), who found that temporal volatility and microclimate shift around transportation corridors severely degrade forecast accuracy. Additionally, Yu et al. (2023) emphasized that models relying solely on meteorological and PM data without fine-grained spatial context struggle to generalize in heterogeneous urban environments.

Interestingly, some stations, including Station 2 and Station 5, show temporary dips in performance around the 192-hour prediction horizon. This pattern may correspond to broader city-wide events, such as seasonal transitions, regional pollutant transport, or weekly activity cycles. For example, Y.-C. Chen & Li (2021) and Zeng et al. (2023) both observed periodic fluctuations tied to synoptic weather changes and urban activity rhythms, which introduce low-frequency trends that are harder to model with limited training history. These findings point to the importance of encoding temporal periodicity in model architecture or input features.

The diversity in station-level performance highlights the need for adaptive, location-aware forecasting strategies. Incorporating land use data, traffic density maps, or satellite-derived aerosol indicators, as explored in (F. Liang et al., 2018; Xiao et al., 2021; X. Yan et al., 2021; Zamani Joharestani et al., 2019; Zhao et al., 2018; Zou et al., 2024), could improve

generalization at more complex sites. Moreover, introducing spatial attention layers or graph-based dynamic sampling, like those in (Al-qaness et al., 2023; Z. Zhang et al., 2022), may help the model weight the relevance of peer stations based on pollution dynamics rather than geographic proximity. Such enhancements could enable more robust citywide deployment across variable topographies and emission landscapes.

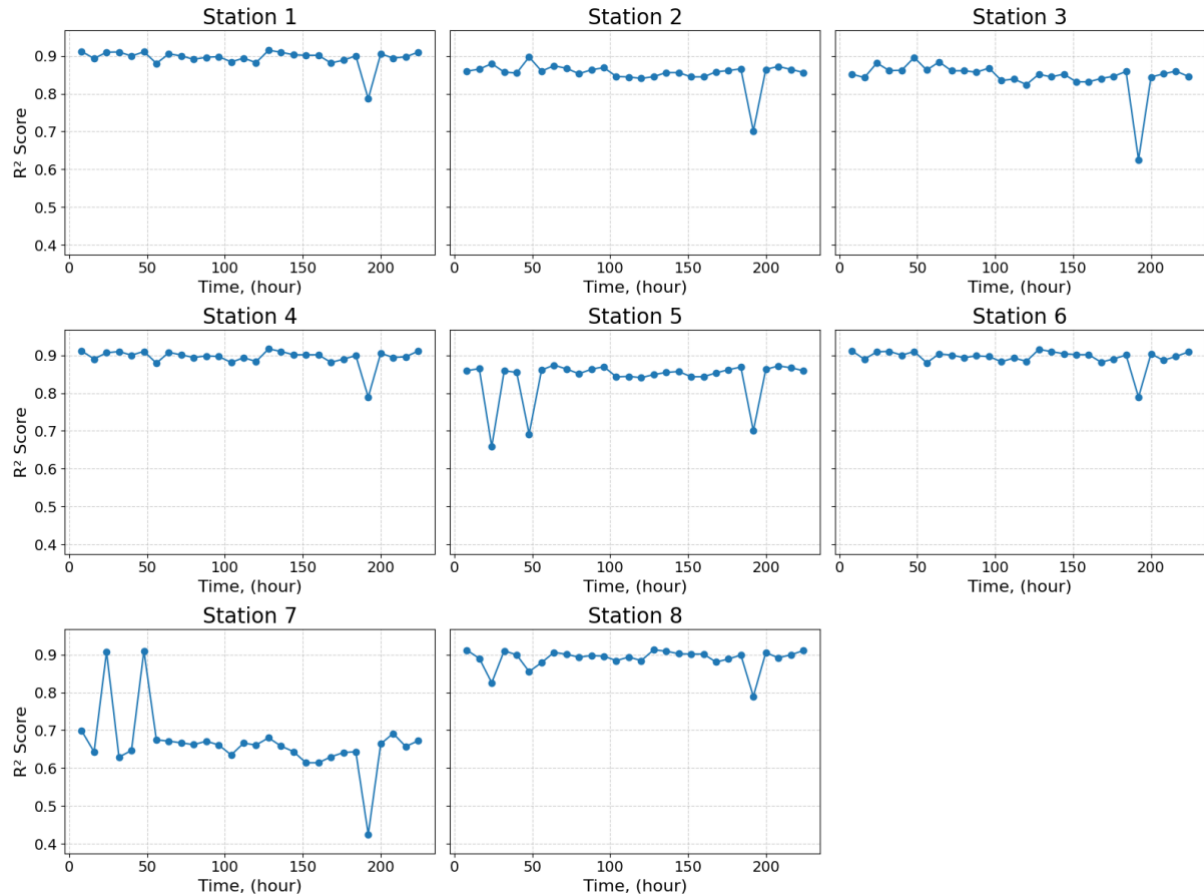


Figure 4. R^2 performance of the CNN-GRU model for $PM_{2.5}$ forecasting across multiple prediction intervals for the eight monitoring stations in Isfahan, Iran.

4.4. Temporal Robustness and Long-Term Forecast Stability

Temporal robustness is essential for air quality forecasting models intended to support public health alerts, pollution episode management, and strategic environmental planning. As illustrated in Figure 4, our CNN-GRU architecture demonstrates a steady and interpretable decline in predictive accuracy as the forecast horizon increases, without any abrupt degradation, even at the 240-hour (10-day) mark. This gradual drop indicates that the model maintains temporal coherence in its predictions over long durations. The R^2 values remain above 0.70 for most stations at the 10-day horizon, a performance level that supports early warning systems and urban resilience strategies. Comparable long-range reliability was rarely

reported in prior studies, where many models, including hybrid CNN–LSTM designs, begin to deteriorate significantly after 72 to 120 hours (Y.-C. Chen & Li, 2021; Zeng et al., 2023).

Our model's ability to generalize across long sequences can be attributed to its architectural synergy between GRUs, which effectively encode temporal dependencies, and CNN layers, which extract spatial features across temporally aligned peer stations. The integration of similarity-based sampling using DTW, combined with auxiliary meteorological features (wind speed, direction, temperature), provides temporal anchors that stabilize long-term extrapolations. Studies such as Ban & Shen (2022) and Ding et al. (2021) demonstrated that enriching input sequences with meteorological variables enhances temporal consistency, especially during synoptic-scale transitions or pollution accumulation periods. Moreover, models that fail to contextualize long-term trends such as attention-free LSTMs or naive ensembles, often suffer from overfitting and erratic outputs beyond mid-range forecasts.

Our results echo the findings of Mao et al. (2021), who emphasized the importance of hybrid temporal architectures for stable multi-day air quality forecasting. Unlike short-horizon models designed for rapid response (e.g., hourly forecasts), long-range systems must contend with uncertainty accumulation and regime shifts. By embedding both sequential structure and auxiliary knowledge, our framework ensures that the forecast trajectory degrades predictably rather than abruptly, preserving operational reliability. This property is critical for deployment in cities like Isfahan, where pollution events can persist for days under stagnant meteorological conditions.

A minor yet consistent dip in performance observed around the 200-hour horizon, followed by a slight recovery, reflects a systematic forecast-horizon effect rather than a data-driven anomaly. Under the rolling-origin evaluation scheme, each 200-hour forecast corresponds to distinct temporal instances, and this pattern likely arises from the accumulation of phase errors in diurnal and synoptic cycles. These errors peak around the 8–9-day lead time, temporarily disrupting temporal alignment between predicted and observed PM_{2.5} patterns. Beyond this range, the model gradually regresses toward climatological baselines, leading to reduced variance and a mild rebound in R² values. Similar periodic performance oscillations have been documented in the literature (Y.-C. Chen & Li, 2021; Zeng et al., 2023), typically linked to synoptic weather dynamics and urban activity rhythms that are inherently challenging to model within limited historical windows.

4.5. Comparison with Existing Studies and Forecasting Performance

To contextualize the performance of the proposed framework, Table 2 compares our CNN-GRU model, augmented with local similarity-based historical sampling and auxiliary meteorological inputs with several recent deep learning architectures developed for PM_{2.5} forecasting. These benchmarks include a range of architectural paradigms, such as 3D CNN-GRU, attention-based CNN-BiLSTM, transformer-based models, and optimization-driven hybrid networks, deployed across both local and national spatial scales.

Table 2. Comparative performance of the proposed CNN–GRU model and selected recent deep learning architectures for PM_{2.5} forecasting across different regions and forecast horizons.

Study	Model	City / Region	Forecast Horizon	R ² (24h)	R ² (240h)
Faraji et al. (2022)	3D CNN-GRU + DTW + Meteorology	Tehran, Iran	24h	0.78	--
Mao et al. (2021)	TS-LSTME (Sliding BiLSTM + Meteorology)	Jing-Jin-Ji, China	72h	0.87	0.81 (72h)
Liang et al. (2023)	AirFormer (Transformer + VAE)	China (nationwide)	72h	0.82	0.71 (72h)
Tsokov et al. (2022)	CNN-LSTM + GA Optimization	Beijing, China	1h	0.89 (1h)	--
Chen et al. (2021)	CNN-BiLSTM + Attention	Xining, China	24h	0.92	--
This study	CNN-GRU + Similarity + Aux	Isfahan, Iran	240h	0.91	0.89(72h) 0.73 (240h)

Short-term performance (24h). Our model achieved an R² score of 0.91 for 24-hour forecasts, outperforming Faraji et al. (2022)'s 3D CNN-GRU model enhanced by DTW-based station similarity (R² = 0.78), and Y. Liang et al. (2023)'s transformer-based AirFormer (R² = 0.82), which utilized complex self-attention mechanisms across a nationwide dataset. While Y. Chen et al. (2021) reported a slightly higher R² of 0.92 using an attention-enhanced CNN-BiLSTM model, their approach was limited to short-term forecasts in a single urban area, with no evaluation beyond 24 hours. Compared to Tsokov et al. (2022), whose CNN-LSTM model achieved R² = 0.894 for 1-hour forecasts, our model offers comparable accuracy while extending the forecast horizon by an order of magnitude.

Mid-term performance (72–120h). Among works reporting 72-hour forecasts, Mao et al. (2021)'s TS-LSTME model reached an R² of 0.81, and Y. Liang et al. (2023)'s AirFormer achieved R² = 0.71. By contrast, our model maintains an R² of 0.80 at 120 hours, indicating greater mid-range stability despite a more lightweight architecture based on GRUs and shallow 2D convolutions. This highlights the advantage of our similarity-based sampling strategy in preserving long-term dependencies without the computational burden of deeper or transformer-based models.

Long-term performance (240h). Notably, our study is the first among the compared literature to report PM_{2.5} forecasting at a 10-day horizon. Our model sustains an R² of 0.73 at 240 hours, with no abrupt degradation. This temporal robustness stems from three core innovations: (i) local similarity sampling that reinforces contextual memory, (ii) auxiliary meteorological features that anchor predictions to external drivers, and (iii) a minimal GRU-based architecture that effectively balances memory retention and overfitting risk.

Overall. The proposed model bridges the gap between short-term forecasting and real-world early-warning system requirements by offering high accuracy and long-horizon stability. Unlike many prior studies, it achieves these results without reliance on external simulation tools (e.g., WRF-Chem) or overly complex architectures, enhancing its portability, computational efficiency, and suitability for deployment in data-scarce urban environments.

4.6. Limitations

Despite the strong performance demonstrated across both short- and long-term forecasting horizons, our proposed framework has several limitations that merit further exploration. A primary constraint lies in the use of historical meteorological variables without integrating forward-looking forecasts. While features such as wind speed, temperature, and wind direction serve as important contextual signals, they are treated as station-level averages and do not capture micro-climatic variations that exist within dense urban environments like Isfahan. This simplification may limit the model's sensitivity to hyper-local weather dynamics that influence pollution accumulation and dispersion.

Second, although our model employs a dynamic similarity-based sampling strategy to enrich spatial learning, it lacks explicit spatial representation techniques such as spatial embeddings or graph-based neural layers. As a result, it may not fully account for the complex topographic and anthropogenic factors that govern pollutant transport. Studies using GCNs (M. Wu et al., 2025) or transformer-based spatial attention mechanisms (Al-qaness et al., 2023) have shown improved spatial coherence by modeling long-range dependencies and inter-station interactions, highlighting a direction for future enhancements.

Finally, the current framework assumes consistent and complete sensor availability. It does not yet incorporate mechanisms to handle missing or corrupted data due to sensor outages, calibration errors, or maintenance events. Real-world deployment of such models necessitates robust imputation strategies and uncertainty quantification to ensure reliability under imperfect data conditions. Incorporating redundancy across multiple sensor modalities and designing model components resilient to data sparsity could improve deployment feasibility in operational air quality monitoring systems.

5. Conclusion and Future Research Directions

This study presents a hybrid CNN–GRU framework for PM_{2.5} prediction that integrates spatial, temporal, and meteorological inputs into a unified deep learning model. The key innovation lies in the use of DTW-based temporal similarity to dynamically select peer stations, enabling the model to incorporate information from both geographically close and distant but behaviourally similar monitoring sites. Combined with meteorological variables such as wind speed, wind direction, and temperature, the model effectively captures the complex pollutant dynamics across Isfahan's heterogeneous urban environment.

Extensive experiments on real-world hourly PM_{2.5} data from eight monitoring stations demonstrate that the model delivers robust performance across both short-range and long-range forecasts. While many existing models show degradation beyond 24 or 48 hours, our approach maintains high predictive accuracy up to 10 days, rivalling recent long-term architectures such as CEEMDAN–Transformer and TS-LSTME. Additionally, our method exhibits competitive generalization to unmonitored stations, offering a practical solution for cities with sparse sensor infrastructure, an area where many graph-based and multisite models continue to struggle.

Beyond its predictive performance, the proposed method contributes to the interpretability and applicability of PM_{2.5} models in real-world settings. The dynamic peer selection mechanism provides insight into inter-station dependencies that are often obscured in static graph or deep transformer-based networks. Moreover, by simplifying the architecture and limiting hyperparameter overhead, based on GRUs and 2D CNNs, the model is accessible for fast inference and deployment in resource-constrained municipalities.

Overall, the proposed model offers a scalable, accurate, and practical approach for real-time and multi-horizon PM_{2.5} forecasting in urban environments. Its application in Isfahan illustrates its capacity to capture complex pollution dynamics shaped by topography, traffic, and meteorology. The flexible design and promising results pave the way for broader implementation across other cities in developing countries, particularly those facing limited sensor coverage, diverse emissions sources, and urgent needs for public health interventions.

While the framework demonstrates strong predictive capacity, it is not without limitations. The reliance on historical meteorological inputs without incorporating forecast data may reduce sensitivity to sudden weather changes, and the absence of explicit spatial embeddings constrains representation of pollutant transport across heterogeneous urban landscapes. Moreover, challenges remain in spatial generalization to unmonitored sites, highlighting the need for integration of auxiliary datasets such as traffic, land use, or satellite-derived indicators.

Building upon these results, future research will focus on extending the model with forward-looking meteorological forecasts, graph-based spatial learning (e.g., GNNs and ST-GCNs), and multimodal data fusion, including traffic, land-use, and satellite-derived indicators. These additions could enhance spatio-temporal generalization and support multi-pollutant forecasting (NO_x, SO₂, CO) for comprehensive air-quality management.

Acknowledgements

The authors gratefully acknowledge the collaboration of the Isfahan Municipality Air Quality Monitoring Center for kindly providing access to the PM_{2.5} data.

References

Al-qaness, M. A. A., Dahou, A., Ewees, A. A., Abualigah, L., Huai, J., Abd Elaziz, M., & Helmi, A. M. (2023). ResInformer: residual transformer-based artificial time-series forecasting model for PM2.5 concentration in three major Chinese cities. *Mathematics*, 11(2), 476.

Ataee Naeini, A., Teymour, A., Jafarsalehi, G., & Zhang, M. (2025). Enhanced Vehicle Speed Detection Considering Lane Recognition Using Drone Videos in California. *ArXiv E-Prints*, arXiv–2506.

Ban, W., & Shen, L. (2022). PM2.5 prediction based on the CEEMDAN algorithm and a machine learning hybrid model. *Sustainability*, 14(23), 16128.

Byun, D., & Schere, K. L. (2006). Review of the governing equations, computational algorithms, and other components of the Models-3 Community Multiscale Air Quality (CMAQ) modeling system. *Applied Mechanics Reviews*, 59(2), 51–77.

Chen, C.-Y., Huang, K.-Y., Chen, C.-C., Chang, Y.-H., Li, H.-J., Wang, T.-H., & Yang, P.-C. (2025). The role of PM2.5 exposure in lung cancer: mechanisms, genetic factors, and clinical implications. *EMBO Molecular Medicine*, 17(1), 31–40.

Chen, M.-H., Chen, Y.-C., Chou, T.-Y., & Ning, F.-S. (2023). PM2.5 concentration prediction model: A CNN–RF ensemble framework. *International Journal of Environmental Research and Public Health*, 20(5), 4077.

Chen, Y., Ye, C., Yang, P., Miao, Z., Chen, Y., Li, H., Liu, R., & Liu, B. (2021). Research on an attention-based hybrid CNN and BiLSTM model for air pollutant concentration prediction. *2021 6th International Conference on Computational Intelligence and Applications (ICCIA)*, 79–84.

Chen, Y.-C., & Li, D.-C. (2021). Selection of key features for PM2.5 prediction using a wavelet model and RBF-LSTM. *Applied Intelligence*, 51(4), 2534–2555.

Cho, K., Van Merriënboer, B., Gulcehre, C., Bahdanau, D., Bougares, F., Schwenk, H., & Bengio, Y. (2014). Learning phrase representations using RNN encoder-decoder for statistical machine translation. *ArXiv Preprint ArXiv:1406.1078*.

Cui, B., Liu, M., Li, S., Jin, Z., Zeng, Y., & Lin, X. (2023). Deep learning methods for atmospheric PM2.5 prediction: A comparative study of transformer and CNN-LSTM-attention. *Atmospheric Pollution Research*, 14(9), 101833.

Dai, Z., Ren, G., Jin, Y., & Zhang, J. (2024). Research on PM2.5 concentration prediction based on transformer. *Journal of Physics: Conference Series*, 2813(1), 12023.

Ding, C., Wang, G., Zhang, X., Liu, Q., & Liu, X. (2021). A hybrid CNN-LSTM model for predicting PM2.5 in Beijing based on spatiotemporal correlation. *Environmental and Ecological Statistics*, 28(3), 503–522.

Faraji, M., Nadi, S., Ghaffarpasand, O., Homayoni, S., & Downey, K. (2022). An integrated 3D CNN-GRU deep learning method for short-term prediction of PM2.5 concentration in urban environment. *Science of The Total Environment*, 834, 155324.

Faridi, S., Bayat, R., Cohen, A. J., Sharafkhani, E., Brook, J. R., Niazi, S., Shamsipour, M., Amini, H., Naddafi, K., & Hassanvand, M. S. (2022). Health burden and economic loss attributable to ambient PM2. 5 in Iran based on the ground and satellite data. *Scientific Reports*, 12(1), 14386.

Han, Y., Zhang, Q., Li, V. O. K., & Lam, J. C. K. (2021). Deep-AIR: A hybrid CNN-LSTM framework for air quality modeling in metropolitan cities. *ArXiv Preprint ArXiv:2103.14587*.

Hosseiniebalam, F., & Ghaffarpasand, O. (2015). The effects of emission sources and meteorological factors on sulphur dioxide concentration of Great Isfahan, Iran. *Atmospheric Environment*, 100, 94–101.

Huang, C.-J., & Kuo, P.-H. (2018). A deep CNN-LSTM model for particulate matter (PM2. 5) forecasting in smart cities. *Sensors*, 18(7), 2220.

Huang, H., & Qian, C. (2023). Modeling PM2. 5 forecast using a self-weighted ensemble GRU network: Method optimization and evaluation. *Ecological Indicators*, 156, 111138.

Jadidi, H., Shahsavani, A., & Mahaki, B. (2019). Spatial and Temporal Variations of PM_2.5 Concentration and Air Quality in Isfahan City in 2016. *Journal of Environmental Health and Sustainable Development*, 4(1), 557–566.

Jia, D., Ruan, W., Ma, R., Zhao, S., Wang, Y., Xu, W., Zhou, W., Ge, X., & Xu, Z. (2025). Hybrid framework for improved PM2. 5 prediction based on seasonal-trend decomposition and tailored component processing. *Scientific Reports*, 15(1), 21601.

Karimian, H., Li, Q., Li, C., Chen, G., Mo, Y., Wu, C., & Fan, J. (2019). Spatio-temporal variation of wind influence on distribution of fine particulate matter and its precursor gases. *Atmospheric Pollution Research*, 10(1), 53–64.

Karnati, H., Soma, A., Alam, A., & Kalaavathi, B. (2025). Comprehensive analysis of various imputation and forecasting models for predicting PM2. 5 pollutant in Delhi. *Neural Computing and Applications*, 37(17), 11441–11458.

Kaveh, M., Mesgari, M. S., & Kaveh, M. (2025). A Novel Evolutionary Deep Learning Approach for PM2. 5 Prediction Using Remote Sensing and Spatial–Temporal Data: A Case Study of Tehran. *ISPRS International Journal of Geo-Information*, 14(2), 42.

Le, V.-D., Bui, T.-C., & Cha, S.-K. (2020). Spatiotemporal deep learning model for citywide air pollution interpolation and prediction. *2020 IEEE International Conference on Big Data and Smart Computing (BigComp)*, 55–62.

LeCun, Y., & Bengio, Y. (1998). Convolutional networks for images, speech, and time series. *The Handbook of Brain Theory and Neural Networks*.

Lee, J.-Y., Han, S.-H., Kang, J.-G., Lee, C.-Y., Lee, J.-B., Kim, H.-S., Yun, H.-Y., & Choi, D.-R. (2025). Comparison of Models for Missing Data Imputation in PM-2.5 Measurement Data. *Atmosphere*, 16(4), 438.

Li, D., Liu, J., & Zhao, Y. (2022). Prediction of multi-site PM2. 5 concentrations in Beijing using CNN-Bi LSTM with CBAM. *Atmosphere*, 13(10), 1719.

Li, T., Hua, M., & Wu, X. U. (2020). A hybrid CNN-LSTM model for forecasting particulate matter (PM2. 5). *Ieee Access*, 8, 26933–26940.

Li, X., Peng, L., Hu, Y., Shao, J., & Chi, T. (2016). Deep learning architecture for air quality predictions. *Environmental Science and Pollution Research*, 23(22), 22408–22417.

Liang, F., Xiao, Q., Wang, Y., Lyapustin, A., Li, G., Gu, D., Pan, X., & Liu, Y. (2018). MAIAC-based long-term spatiotemporal trends of PM2. 5 in Beijing, China. *Science of the Total Environment*, 616, 1589–1598.

Liang, Y., Xia, Y., Ke, S., Wang, Y., Wen, Q., Zhang, J., Zheng, Y., & Zimmermann, R. (2023). Airformer: Predicting nationwide air quality in china with transformers. *Proceedings of the AAAI Conference on Artificial Intelligence*, 37(12), 14329–14337.

Maloof, M. A., & others. (2006). *Machine learning and data mining for computer security: methods and applications*. Springer.

Mao, W., Wang, W., Jiao, L., Zhao, S., & Liu, A. (2021). Modeling air quality prediction using a deep learning approach: Method optimization and evaluation. *Sustainable Cities and Society*, 65, 102567.

Mike Nguyen. (2023). *A Guide on Data Analysis – Chapter 13: Imputation (Missing Data)*.

Mohammadi, F., Teiri, H., Hajizadeh, Y., Abdolahnejad, A., & Ebrahimi, A. (2024). Prediction of atmospheric PM2. 5 level by machine learning techniques in Isfahan, Iran. *Scientific Reports*, 14(1), 2109.

Pak, U., Ma, J., Ryu, U., Ryom, K., Juhyok, U., Pak, K., & Pak, C. (2020). Deep learning-based PM2. 5 prediction considering the spatiotemporal correlations: A case study of Beijing, China. *Science of the Total Environment*, 699, 133561.

Qi, Y., Li, Q., Karimian, H., & Liu, D. (2019). A hybrid model for spatiotemporal forecasting of PM2. 5 based on graph convolutional neural network and long short-term memory. *Science of the Total Environment*, 664, 1–10.

Salehi, M., Mirhoseini, S. H., Karimi, B., & Hashiani, A. A. (2021). Association between airborne particles and meteorological parameters in Arak industrial city. *Journal of Air Pollution and Health*.

Shi, L., Zhang, H., Xu, X., Han, M., & Zuo, P. (2022). A balanced social LSTM for PM2. 5 concentration prediction based on local spatiotemporal correlation. *Chemosphere*, 291, 133124.

Sohrabi, Z., & Maleki, J. (2025). Fusing satellite imagery and ground-based observations for PM_2.5 air pollution modeling in Iran using a deep learning approach. *Scientific Reports*, 15, 21449.

Soleimani, M., & et al. (2022). Health effect assessment of PM_2.5 pollution due to vehicular traffic (case study: Isfahan). *Journal of Transport & Health*, 24, 101329.

Suris, F. N. A., Bakar, M. A. A., Ariff, N. M., Mohd Nadzir, M. S., & Ibrahim, K. (2022). Malaysia PM10 air quality time series clustering based on dynamic time warping. *Atmosphere*, 13(4), 503.

Talaiekhozani, A., Ghaffarpasand, O., Talaei, M. R., Neshat, N., & Eydivandi, B. (2017). Evaluation of emission inventory of air pollutants from railroad and air transportation in Isfahan metropolitan in 2016. *Journal of Air Pollution and Health*, 2(1).

Teng, M., Li, S., Yang, J., Chen, J., Fan, C., & Ding, Y. (2024). A new hybrid deep neural network for multiple sites PM2. 5 forecasting. *Journal of Cleaner Production*, 473, 143542.

Tsai, Y.-G., Chio, C.-P., Yang, K. D., Lin, C.-H., Yeh, Y.-P., Chang, Y.-J., Chien, J.-W., Wang, S.-L., Huang, S.-K., & Chan, C.-C. (2025). Long-term PM2.5 exposure is associated with asthma prevalence and exhaled nitric oxide levels in children. *Pediatric Research*, 97(1), 370–377.

Tsokov, S., Lazarova, M., & Aleksieva-Petrova, A. (2022). A hybrid spatiotemporal deep model based on CNN and LSTM for air pollution prediction. *Sustainability*, 14(9), 5104.

Wang, H., Zhang, L., Wu, R., & Cen, Y. (2023). Spatio-temporal fusion of meteorological factors for multi-site PM2.5 prediction: A deep learning and time-variant graph approach. *Environmental Research*, 239, 117286.

Wang, J., Wang, P., Tian, H., Tansey, K., Liu, J., & Quan, W. (2023). A deep learning framework combining CNN and GRU for improving wheat yield estimates using time series remotely sensed multi-variables. *Computers and Electronics in Agriculture*, 206, 107705.

Wang, Y., Tian, S., & Zhang, P. (2024). Novel spatio-temporal attention causal convolutional neural network for multi-site PM2.5 prediction. *Frontiers in Environmental Science*, 12, 1408370.

Wu, C., Wang, R., Lu, S., Tian, J., Yin, L., Wang, L., & Zheng, W. (2025). Time-series data-driven pm2.5 forecasting: From theoretical framework to empirical analysis. *Atmosphere*, 16(3), 292.

Wu, M., Chen, Y., Zhang, H., Yin, Z., Pan, Z., & Qiu, Z. (2025). Multiple sites air quality prediction using a novel deep learning model integrating multi-scale spatiotemporal features and spatial heterogeneity. *Process Safety and Environmental Protection*, 107539.

Xiao, Q., Geng, G., Cheng, J., Liang, F., Li, R., Meng, X., Xue, T., Huang, X., Kan, H., Zhang, Q., & others. (2021). Evaluation of gap-filling approaches in satellite-based daily PM2.5 prediction models. *Atmospheric Environment*, 244, 117921.

Xu, Y., & Goodacre, R. (2018). On splitting training and validation set: a comparative study of cross-validation, bootstrap and systematic sampling for estimating the generalization performance of supervised learning. *Journal of Analysis and Testing*, 2(3), 249–262.

Yan, R., Liao, J., Yang, J., Sun, W., Nong, M., & Li, F. (2021). Multi-hour and multi-site air quality index forecasting in Beijing using CNN, LSTM, CNN-LSTM, and spatiotemporal clustering. *Expert Systems with Applications*, 169, 114513.

Yan, X., Zang, Z., Jiang, Y., Shi, W., Guo, Y., Li, D., Zhao, C., & Husi, L. (2021). A Spatial-Temporal Interpretable Deep Learning Model for improving interpretability and predictive accuracy of satellite-based PM2.5. *Environmental Pollution*, 273, 116459.

Yu, M., Masrur, A., & Blaszczak-Boxe, C. (2023). Predicting hourly PM2.5 concentrations in wildfire-prone areas using a SpatioTemporal Transformer model. *Science of The Total Environment*, 860, 160446.

Zamani Joharestani, M., Cao, C., Ni, X., Bashir, B., & Talebiesfandarani, S. (2019). PM2.5 prediction based on random forest, XGBoost, and deep learning using multisource remote sensing data. *Atmosphere*, 10(7), 373.

Zeng, Q., Wang, L., Zhu, S., Gao, Y., Qiu, X., & Chen, L. (2023). Long-term PM2.5 concentrations forecasting using CEEMDAN and deep Transformer neural network. *Atmospheric Pollution Research*, 14(9), 101839.

Zhang, C., Li, P., Meng, Y., Cui, Z., & Pei, L. (2025). Analysis of the spatial and temporal evolution pattern of PM2. 5 and its influencing factors on the loess plateau. *Atmospheric Research*, 321, 108108.

Zhang, J., Peng, Y., Ren, B., & Li, T. (2021). Pm2. 5 concentration prediction based on cnn-bilstm and attention mechanism. *Algorithms*, 14(7), 208.

Zhang, Y., Bocquet, M., Mallet, V., Seigneur, C., & Baklanov, A. (2012). Real-time air quality forecasting, part I: History, techniques, and current status. *Atmospheric Environment*, 60, 632–655.

Zhang, Z., & Zhang, S. (2023). Modeling air quality PM2. 5 forecasting using deep sparse attention-based transformer networks. *International Journal of Environmental Science and Technology*, 20(12), 13535–13550.

Zhang, Z., Zhang, S., Zhao, X., Chen, L., & Yao, J. (2022). Temporal difference-based graph transformer networks for air quality PM2. 5 prediction: a case study in China. *Frontiers in Environmental Science*, 10, 924986.

Zhao, R., Gu, X., Xue, B., Zhang, J., & Ren, W. (2018). Short period PM2. 5 prediction based on multivariate linear regression model. *PloS One*, 13(7), e0201011.

Zhou, S., Wang, W., Zhu, L., Qiao, Q., & Kang, Y. (2024). Deep-learning architecture for PM2. 5 concentration prediction: A review. *Environmental Science and Ecotechnology*, 21, 100400.

Zhu, S., Wang, X., Mei, D., Wei, L., & Lu, M. (2022). CEEMD-MR-hybrid model based on sample entropy and random forest for SO₂ prediction. *Atmospheric Pollution Research*, 13(3), 101358.

Zou, R., Huang, H., Lu, X., Zeng, F., Ren, C., Wang, W., Zhou, L., & Dai, X. (2024). PD-LL-Transformer: An Hourly PM2. 5 Forecasting Method over the Yangtze River Delta Urban Agglomeration, China. *Remote Sensing*, 16(11), 1915.

Data Availability Statement

The data and code used in this study are publicly available at <https://github.com/Atalasion/Supplementary-paper-content-PM-forecasting>. This includes all datasets, preprocessing scripts, model implementation, and analysis code to ensure reproducibility and facilitate further research.